Applied Physics A (2019) 125:149
https://doi.org/10.1007/s00339-019-2443-x

Applied Physics A
Materials Science & Processing

Ultrabroadband metamaterial absorbers based on ionic liquids

Fulong Yang[1,2] · Jianhao Gong[1] · E. Yang[1] · Yongji Guan[1] · Xiaodong He[1] · Shimin Liu[3] · Xiaoping Zhang[1] · Youquan Deng[3]

Received: 7 November 2018 / Accepted: 24 January 2019

Abstract
An ultrabroadband metamaterial absorber (MMAs) based on room temperature ionic liquids (ILs) and composed entirely of cations and anions was proposed and analyzed in the microwave regimen. The dielectric permittivity of the ILs [EMIm] $[N(CN)_2]$ was investigated from 0.5 to 50 GHz; the loss tangent tanδ of [EMIm] $[N(CN)_2]$ declines from 5.91 to 0.34, which implies a high dielectric loss of microwaves. To further improve the impedance matching over a wide band, the ILs [EMIm] $[N(CN)_2]$ were injected in a periodic photopolymer cylindrical array fabricated via 3D printing. We numerically and experimentally demonstrate that this absorber shows over 90% absorption at 9.26–49 GHz when the incident angle is 45° with a relative bandwidth as high as 134.6%. Versus water-based MMAs, the proposed absorber shows more than twice the absorption bandwidth. Mechanistic investigations show that the ultrabroadband absorption characteristics of the ILs-based MMAs mainly contribute to IL dispersion and electromagnetic resonance. Furthermore, the electromagnetic wave energy loss is mainly due to the high-dielectric loss of ILs [EMIm] $[N(CN)_2]$.

1 Introduction

Electromagnetic (EM) metamaterials (MMs) have permittivity and permeability that are tunable via artificial periodic structural arrays and have been used widely in science and engineering [1–4]. Examples include invisibility cloaks [5–7], perfect MM absorbers [8–12], super lens [13, 14], and polarizers [15, 16]. Thus, MM absorbers (MMAs) are attracting increasing attention with applications in solar cells [17, 18], image systems [19, 20], sensor [21] and photodetectors [22, 23]. The first MMAs were proposed by Landy et al. in 2008 followed by many other iterations.

✉ Xiaoping Zhang
zxp@lzu.edu.cn

✉ Youquan Deng
ydeng@licp.cas.cn

[1] School of Information Science and Engineering, Lanzhou University, Lanzhou 730000, China

[2] Key Laboratory of Gansu Advanced Control for Industrial Processes, College of Electrical and Information Engineering, National Experimental Teaching Center of Electrical and Control Engineering, Lanzhou University of Technology, Lanzhou 730000, China

[3] Centre for Green Chemistry and Catalysis, Lanzhou Institute of Chemical Physics, CAS, Lanzhou 730000, China

MMAs consist of three layers: a patterned metal layer that minimizes reflection via impedance matching, a dielectric layer, and a continuous metal layer for blocking transmission. Versus traditional absorbers, MMAs are slimmer, more affordable, easier to design, and have nearly perfect absorption. However, they are limited by narrow absorption bandwidths due to their strong electric and magnetic resonances.

Several methods have been used to broaden the absorption bandwidth of MMAs and overcome these limitations of narrow bandwidth. A single-layer absorber structure composed of multi-resonance units with differing geometric dimensions was used to extend the bandwidth [24–26]. Alternatively, a multi-layered structure used with vertically stacking of multiple different-sized metallic resonance structures to enhance the absorption bandwidth [27–29]. Several other bandwidth-enhancement approaches include lumped element loading and frequency tunable techniques [30–32]. However, these methods are limited in the practical application of MMAs due to fabrication difficulties.

More recently, water was used as a medium to design MMAs and included absorbers based on its dispersion features [33–38]. In contrast to conventional solid-material-based MMAs, liquid-based MMAs are easily reconfigurable and tunable with low cost, wide frequency bands, and small densities. Challenges include their volatile nature, poor thermal stability, and easy vaporization/condensation. Therefore,

Published online: 01 February 2019

novel liquid materials are needed for metamaterial absorbers; ILs are an ideal alternative.

Room-temperature ionic liquids (ILs) are a novel class of versatile solvents and soft materials with unique physicochemical properties, including negligible vapor pressure, wide liquid range, intrinsic ionic conductivity, and acceptable electrochemical stability and environmental friendliness [39–41]. The most important characteristic of ILs is that their properties can be significantly tuned by changing their combination of ions—this makes them "designable materials." Our group recently realized wideband MMAs using ILs; strong absorption of microwaves above 90% was achieved in the 8.4–29.0 GHz range; this confirms the feasibility of using ILs for the design of ultra-material absorbers [42].

In this paper, we presented an ILs-based ultrabroadband all-dielectric MMAs at microwave frequencies. The IL ([EMIm] $[N(CN)_2]$) was injected into a periodic photopolymer cylindrical array by 3D printing technology. By introducing a media match layer and adjusting the unit cell cylinder sizes, the effective impedance of the composite structure can be markedly tuned to match the free space. The simulations and experiments show that the absorber can work in an ultra-wideband regimen reaching 39.74 GHz with more than 90% absorptivity because of the dispersion feature of ILs [EMIm] $[N(CN)_2]$. The absorber is valid over a wide range of incident and polarization angles.

2 Design and simulation

2.1 Unit cell and ILs choose

The unit cell configuration of the ILs-based broadband MMAs a four-layer structure are consisted of the top dielectric cover, cylinder dielectric, dielectric substrate, and metal layers. The ILs [EMIM] $[N(CN)_2]$ are then injected into the cylinder dielectric as shown in Fig. 1a. To optimize the impedance characteristics, a multilayer absorbing structure is constructed by introduced a top dielectric layer with the dielectric parameter ($\varepsilon = 3$) smaller than that of ILs. As the electromagnetic waves enter the top dielectric layer and ILs layer in turn from air, the electromagnetic parameters of medium gradually increase, so that the incident electromagnetic waves can be effectively absorbed [43, 44]. The thicknesses of the top dielectric cover, ILs, and the dielectric substrate are defined as *b, d*, and *t*, respectively. The period, radius, and thicknesses of the cylinder dielectric array are defined as *p, r*, and *k*, respectively (Fig. 1b).

The ILs [EMIm][$N(CN)_2$], [BMIm][$N(CN)_2$], [EMIm][BF_4] and [BMIm][BF_4] were synthesized according to the literature [45] with purity > 99%. Before measurements, the ILs were carefully dried under vacuum at ~40 °C for at least 7 days with water contents < 40 ppm as determined by colorimetric Karl Fischer titration. The complex permittivities [$\varepsilon(\omega)$] were measured via a probe method with an Agilent vector network analyzer N5247A in the frequency range of 0.5–50 GHz. Figure 2a shows that the ILs [EMIm] $[N(CN)_2]$ have relatively low $\varepsilon'(\omega)$ from 4.76 to 13.15, and the loss tangent ($\tan\delta = \varepsilon''(\omega)/\varepsilon'(\omega)$) are quite large (0.34–5.91). This implies a high dielectric loss of microwaves. The combination variation of cations and anions for ILs makes them display different dielectric properties [46], which has a significant impact on the performance of the metamaterial absorber. It is found that the absorption performance, including absorption wideband and peaks frequency change obviously as various ILs (i.e., [EMIm][$N(CN)_2$], [BMIm][$N(CN)_2$], [EMIm][BF_4], [BMIm][BF_4]) are filled in the cylinder (Fig. 2b). Considering that [EMIm][$N(CN)_2$]-based metamaterial absorber exhibits the most wide wideband (> 90% absorptivity), it is employed as the object in our following work.

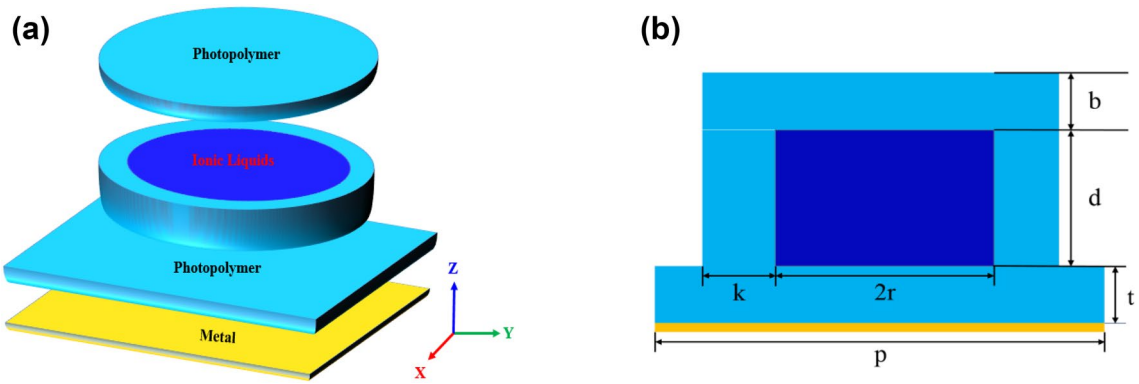

Fig. 1 **a** 3D schematic diagram and **b** the side view of the MMA

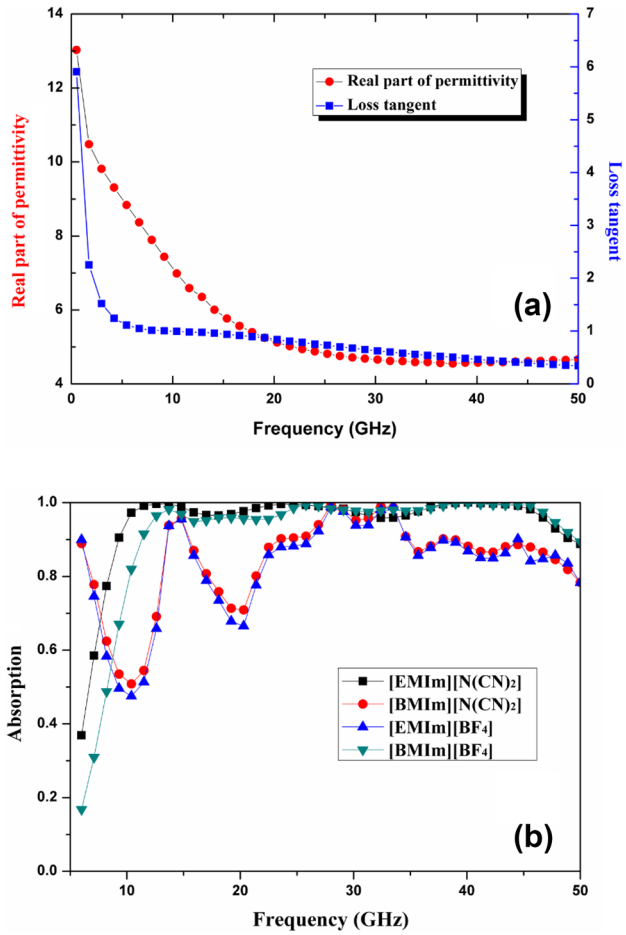

Fig. 2 **a** Real part of permittivity and loss tangent of ILs [EMIm][$N(CN)_2$]. **b** Effect of types of ILs on MMAs absorption performance ($b=1$ mm, $d=2.2$ mm, $t=1$ mm, $r=5.5$ mm, $k=1$ mm and $p=14$ mm)

2.2 Numerical simulation and discussion

Based on the finite integration technique, numerical simulations were performed with using the full-wave electromagnetic simulation software CST Microwave Studio^{TM}. The unit cell was used, and the incident electromagnetic wave was assumed to propagate along the negative z-direction. In our simulation, the thickness and electric conductivity of the bottom copper layer is 36 μm and 5.8×10^7 S/m, respectively; the permittivity of the dielectric is 3. The absorption is calculated from the reflection coefficient because of bottom metal has an electrically large thickness. The absorbance of the absorber can be defined as $A(\omega)=1-R(\omega)-T(\omega)$, where$A(\omega)$, $R(\omega)$and $T(\omega)$ are the absorbance, reflectance, and transmittance as functions of frequency ω, respectively. The absorbance is determined by $A(\omega)=1-R(\omega)$ because the structure is backed by a copper layer, and the transmittance of the EM wave is zero.

Next, we discuss the effect of the structural parameters on the absorption curves. Keeping other structural parameters of the absorber unchanged ($d=2.2$ mm, $t=1$ mm, $r=5.5$ mm, $k=1$ mm, $p=14$ mm), the absorption curves with the top medium thickness of b changed from 0 to 1.6 mm. The simulation results of absorption performance are given in Fig. 3a. When there is no the top medium, the absorption bandwidth is narrow from 10 to 33.06 GHz. The absorption performance become excellent with b increases from 0 to 1 mm, but it become worse as the thickness increases from 1 to 1.6 mm. This perfect absorption can be understood via impedance matching—the top medium layer b is an antireflection film.

Figure 3b shows changes in the electromagnetic wave absorption spectrum with various height of ILs d from 1.4 to 3.0 mm. When the height is 1.4 mm, the broadband absorption characteristics are separated at 39.1 GHz. When the height of IL is more than 1.8 mm, >90% absorption over a wide frequency range is observed—the absorption spectrum shifts to a low frequency domain while d gradually increases. When d becomes 1.4, 1.8, 2.2, 2.6 and 3.0 mm, the absorption edge frequency (the first frequency with absorptivity more than 90%) is gradually transferred to a low frequency domain of 11.50, 10.58, 10.29, 9.62, and 7.95 GHz. This results from the longer path of the longitudinal currents induced in the ILs. Similar to the absorption variation with changing parameter d, the stopband edge frequency is gradually transferred to a low frequency domain when the values of the bottom medium thickness t are 0.8–1.6 mm (Fig. 3c).

The radius (r) and unit period (p) of the IL cylinder are also important parameters that affect the absorption performance. The similar variation tendency of the absorption is formed when changing r and p. Figure 4a, b shows the absorption properties of the ILs-MMA with r from 4 to 6 mm and p from 13 to 17 mm. The absorption performance of the ILs-MMA improves as r increases and p decreases. The absorption edge frequency moves to a low frequency domain because of the impedance mismatch and the longer induced current paths. The simulated results of absorption with different thicknesses of cylinder dielectric k are depicted in Fig. 4c. As k increases from 0.25 to 1.25 mm, the absorption low-edge frequency remains constant, and the absorption upper edge frequency gradually increases. These results further confirm the role of geometrical structures in improving the performance of the absorber and indicate the trace of the optimization process.

We also evaluated absorption with different incident angles θ and polarization angles ϕ. Figure 5a demonstrates the results with different incident angles θ ranging from 0° to 60° with a step width of 15°. The absorption is still broad with a 45° incident angle—there is 90% absorption from 10 to 49 GHz. Figure 5b shows the simulated

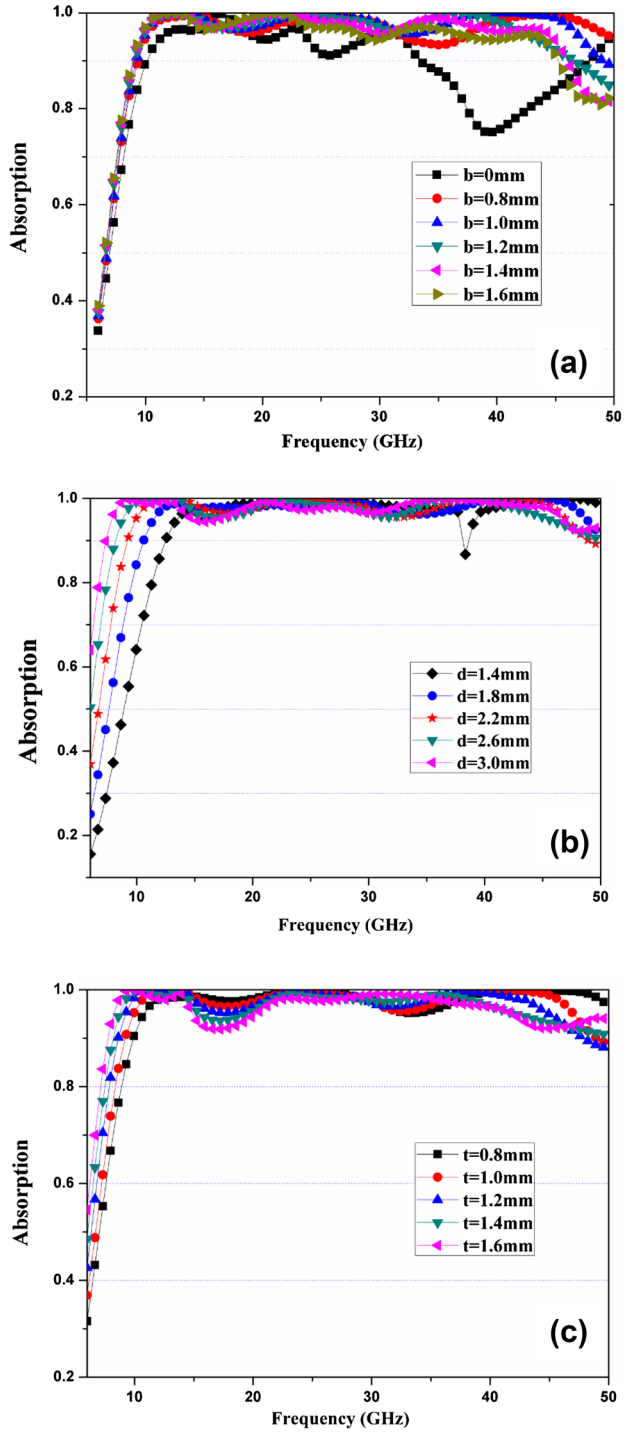

Fig. 3 Influence of geometric parameters on the absorption performance. **a** Thickness of the top layer of *b*, **b** height of the ILs [EMIm][$N(CN)_2$] layer of *d*, **c** thickness of the bottom layer of *t*

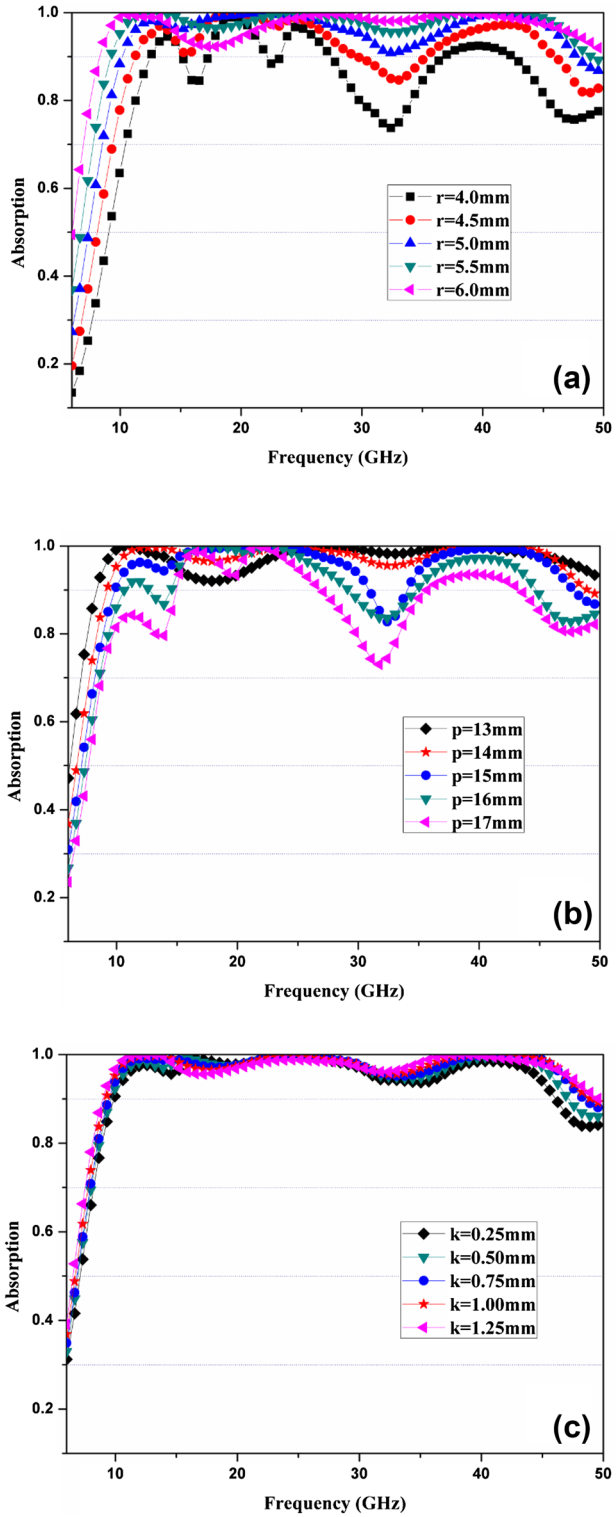

Fig. 4 Absorption performance of the ILMMA at different **a** ILs cylinder radii (*r*), **b** structural periodicity (*p*), and **c** of medium cylinder wall thickness (*k*)

absorption spectra when the polarization angle ϕ varies from 0° to 90° with a step width of 30°; the results show that these ILs-based MMAs are polarization insensitive due to their rotational symmetry. These simulations suggest an ultra-broadband, polarization insensitive, and wide incidence angle MMAs via ILs.

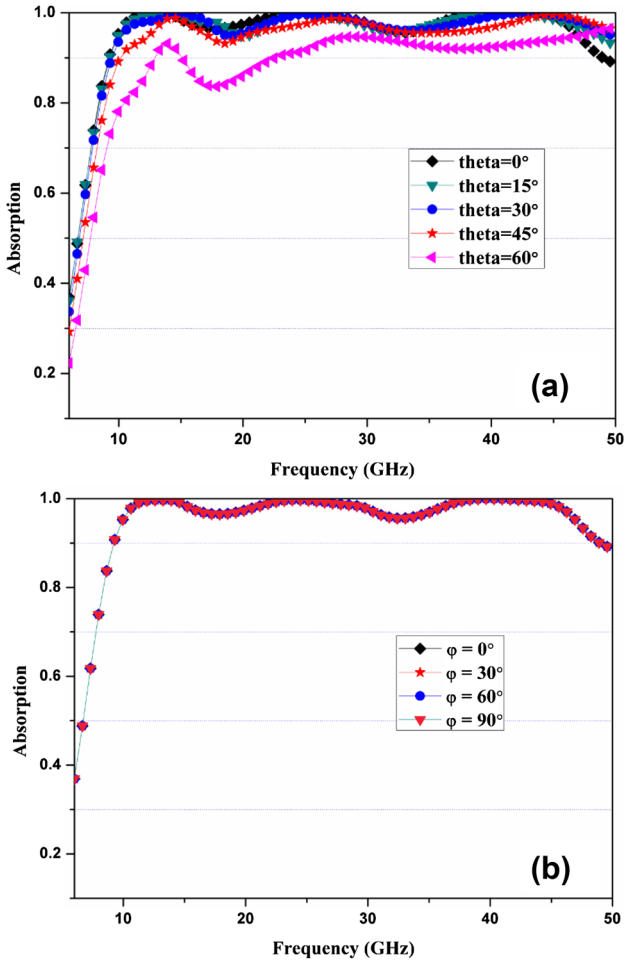

Fig. 5 Absorption performance for different polarization angles (**a**) and incidence angles (**b**)

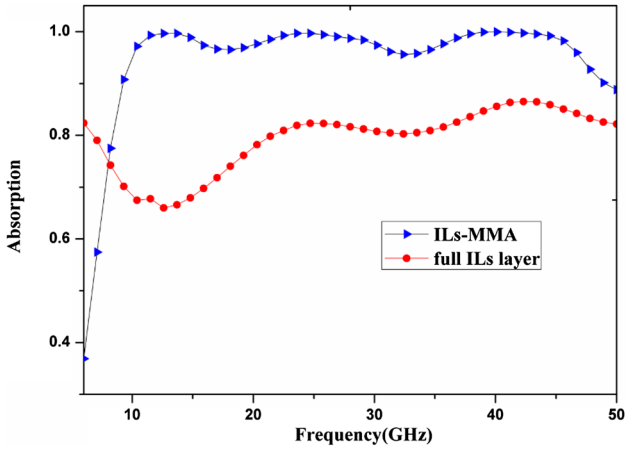

Fig. 6 Absorptivity spectra of the ILs-MMA and the full ILs [EMIm] $[N(CN)_2]$ layer

3 Ultra-wideband characteristics analysis

The optimized geometrical parameters are obtained: $b = 1$ mm, $d = 2.2$ mm, $t = 1$ mm, $r = 5.5$ mm, $k = 1$ mm and $p = 14$ mm. As expected, the broadband absorption could be achieved, with the absorption efficiency over 90% in the frequency range from 9.26 to 49 GHz in Fig. 6. The dielectric properties show that the ILs [EMIm] $[N(CN)_2]$ have high absorption at microwave frequencies. The next goal is to determine if this broadband absorption is predominantly due to the intrinsic high loss of [EMIm] $[N(CN)_2]$. We also considered the case of a full IL [EMIm] $[N(CN)_2]$ layer with the same thickness 4.2 mm as that in the ILs-MMAs. Figure 6 shows that the absorption is less than 86.5% at the frequency band of interest. This indicates a relative weak absorption and implies that the broadband high absorption is mainly due to the localized resonance in the metamaterial with structured ILs resonators.

It is observed that three absorption perks at around 13.3 GHz, 24.2 GHz and 39.9 GHz from the absorption performance of ILs-based ultra-broadband MMAs in Fig. 7. The three absorption peaks indicate three resonances at these frequencies. To fully investigate the intrinsic absorption mechanism of the proposed MMAs, we next investigated the vector distributions of the electric field and magnetic field at resonance frequencies. The loop-shaped electric field lines are near 13.3 GHz (Fig. 7a), which leads to the magnetic resonances [47]. The magnetic field is concentrated in the dielectric substrate and adjacent ILs cylinder units (Fig. 7b). Simultaneously, the magnetic field loops are found at 24.2 GHz and 39.9 GHz corresponding to electric resonances. For the absorption peak at 24.2 GHz, the electric field is localized in the left and right sides of the unit; that at 39.9 GHz is mostly confined to the top dielectric cover. These data show that there are different resonant modes for the three absorption peaks. These resonances in the metamaterial are close to each other in frequency and merge together resulting in broadband absorption. This analysis show that different resonant modes are excited at the absorption peak frequencies—these changes in effective impedance and lead to better impedance matching. We also find that the introduction of the top media cylinder cover limits the energy of the electromagnetic wave and further enlarges the absorption bandwidth.

For a better illustration of the absorption inside the ILs-MMA, the power loss densities at the three resonance frequencies are shown in Fig. 7c. It can be seen that the power loss densities mainly concentrate in ILs layer in all cases, which is simply due to the high-dielectric loss of ILs over the frequency range of interest. However, the absorption schemes are significantly different at these resonance frequencies. At 13.3 GHz, the power loss densities

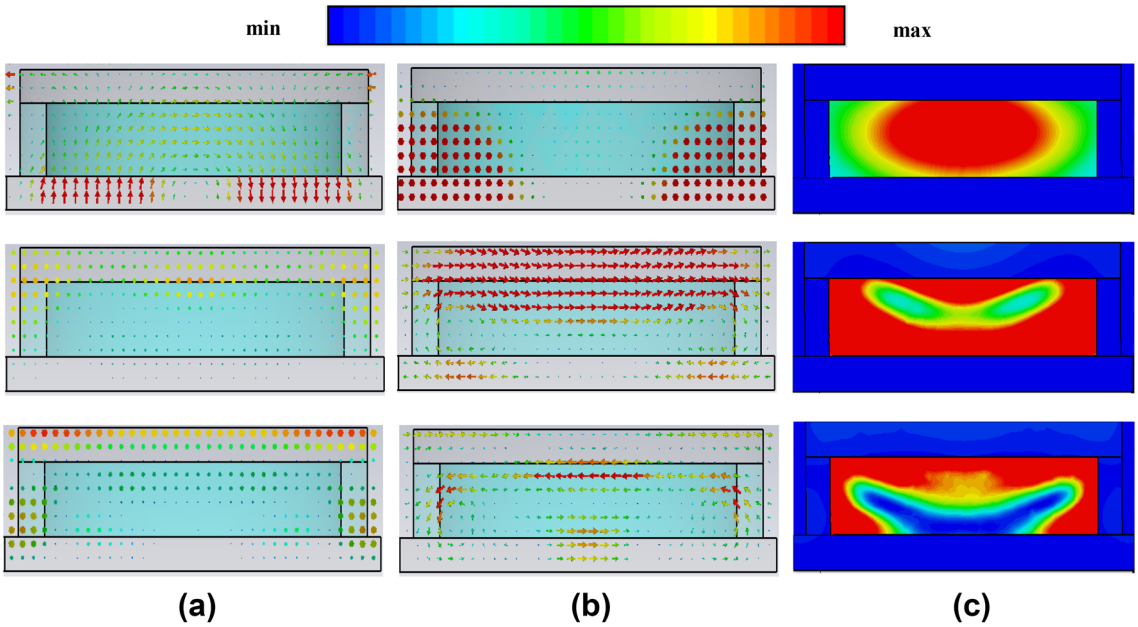

Fig. 7 Vector distributions of the electric field (**a**), magnetic field (**b**), and power loss densities (**c**) of ILs-MMA at resonance frequencies: 13.3 GHz (top), 24.2 GHz (middle), and 39.9 GHz (bottom). The top and middle planes are along the electric field orientation; that on the bottom is the *x*–*z* plane along with the magnetic field orientation

are confined in the center of the ILs. At 24.2 GHz, the majority of power loss densities concentrate at entire the ILs cylinder except for a small part of the interior. At 39.9 GHz, most power loss occurs at the outer and upper edges of ILs cylinder. The combination of these absorption modes leads to an ultra-wideband of high absorption for the ILs-MMA.

4 Experiment results and discussion

To verify the design, we fabricated the proposed absorber containing 13 × 13 units (Fig. 8a) via 3D printing. The top cylindrical dielectric cap and dielectric substrate used the photopolymer DSM Somos 14120. This formed a container for the ILs resonator. A copper foil was placed on the bottom and acted as a metal plate. The ILs [EMIm] [$N(CN)_2$] (0.209 mL) were injected into the dielectric cylinder. The

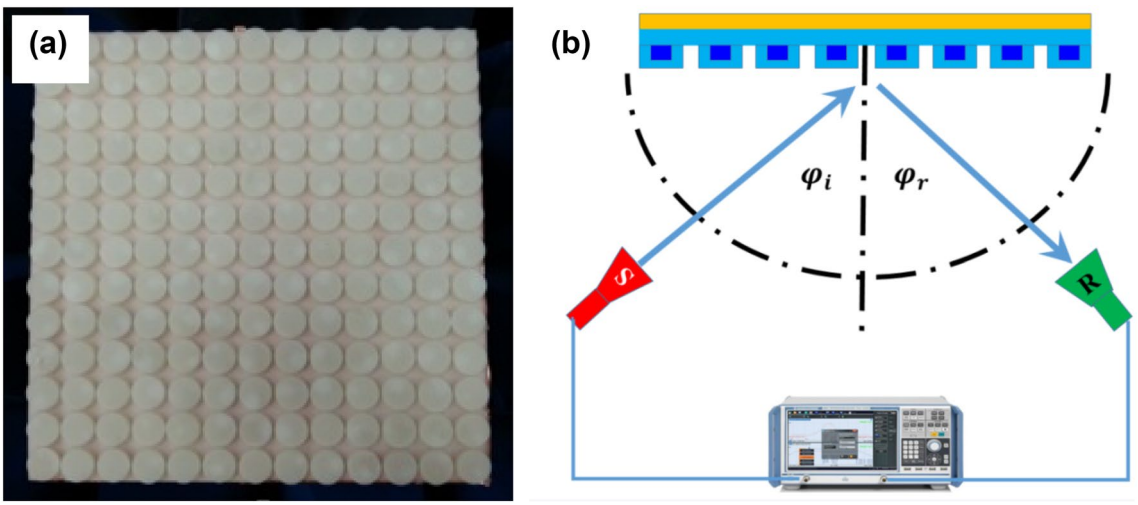

Fig. 8 Photograph of the ILs-MMA prototype (**a**) and experimental set-up for the far-field measurement (**b**)

ILs-MMAs sample was characterized via free space reflection measurements in a microwave anechoic chamber. The measurement system was based on an Agilent Network Analyzer N5247A with a pair of broadband horn antennas (Fig. 8b). The source (tinted in red) could move along the left arc with an incident angle of φ_i. The receiver (tinted in green) could move along the right arc with a reflective angle of $\varphi_r = \varphi_i$. Reflection from a metal plate that was the same size as the prototype was first used for normalization. The absorption was calculated from the measured reflection coefficients of the prototype. The distance between the sample and the antennas was set to ~2.5 m to avoid the near-field effect.

The broadband absorption was simulated and then experimentally demonstrated (Fig. 9). This realized a maximum absorption of 99% with absorption bandwidth of 10.03–50 GHz. The mismatch of the bandwidth was less than 2% between the experimental and simulation results. This was likely due to fabrication error—the slight change in the volume of the ILs was likely due to temperature.

Table 1 compares previous typical liquid-based MMAs to highlight the merits of this approach. The absorption bandwidth of the ILs-MMAs is clearly the widest, and the relative bandwidth is as high as 136.4%.

5 Thermal stability analysis

It is well known that the dielectric properties of ionic liquids are greatly affected by temperature. Therefore, it is necessary to study in detail the temperature dependence of the absorption performance in our ILs-based metamaterial absorber. We measured the dielectric properties of [EMIm][$N(CN)_2$] at the temperature range from 20 to 100 °C using the open-ended coaxial probe method. The results show that, with the increase of temperature, the real parts of permittivity ($\varepsilon'(\omega)$) raises as a whole at 0.5–50 GHz and the loss tangent $\tan\delta = \varepsilon''(\omega)/\varepsilon'(\omega)$ increases clearly, as shown in Fig. 10. Further, the temperature dependence of the absorption performance for the ILs-based metamaterial absorber was studied in detail. Figure 11 shows the absorbing performance of ILs-based metamaterials absorbers with temperature (T)

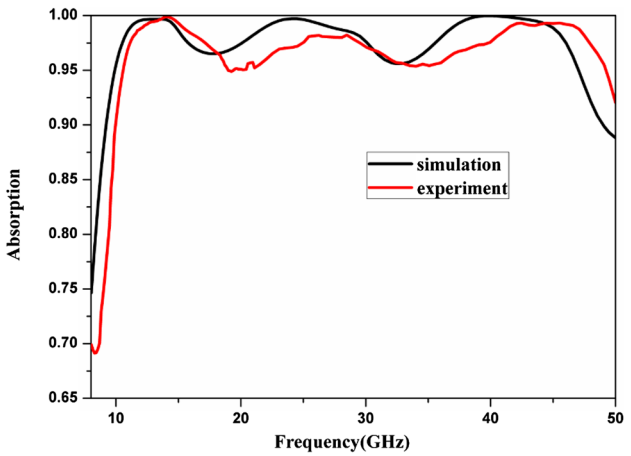

Fig. 9 Simulation and experimental absorption results

Table 1 Comparison on absorption performance between typical liquid-based MMAs in this work and previous works

References	Absorber structure	Absorption bandwidth (GHz)	Relative bandwidth (%)
[33]	Water droplets	8–18	76.9
[34]	Water plate with hole array	12–29.6	84.6
[35]	Water substrate	6.2–19	101.6
[42]	ILs hole array	8.4–29	110.2
This work	ILs cylindrical array	9.26–49	136.4

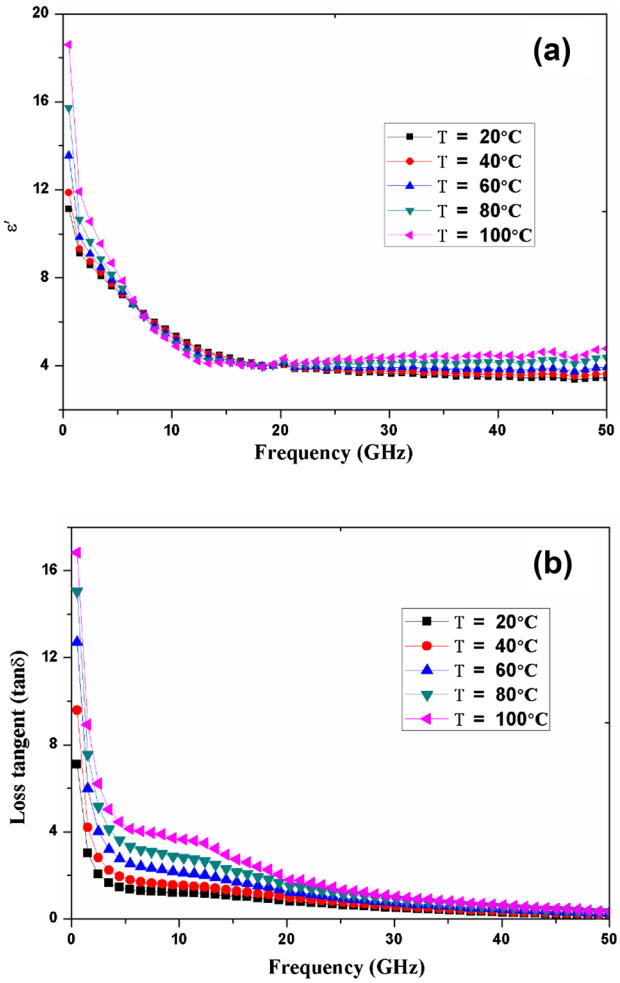

Fig. 10 **a** Real parts and **b** loss tangent (tanδ) of [EMIm][$N(CN)_2$] at different temperatures

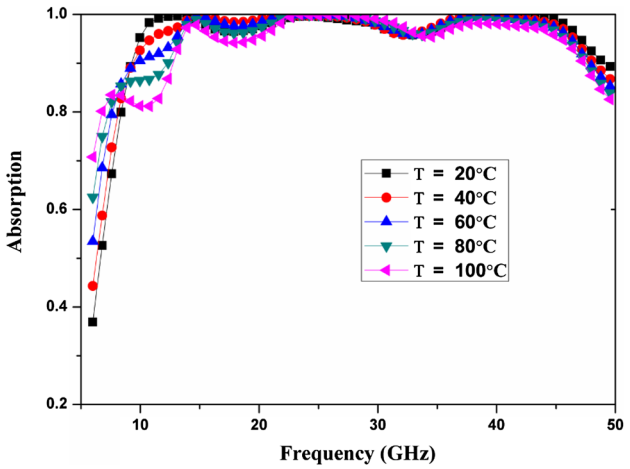

Fig. 11 Effect of temperatures on absorption performance of the ILMMA

from 20 to 100 °C. As the temperature increases, the absorption bandwidth of the absorber becomes slightly narrow. For example, the frequency range with absorption rate over 90% is from 9 to 46.4 GHz when *T* is 20 °C, while the absorption bandwidth is from 11.5 to 45.6 GHz when *T* is 100 °C. The results imply that the absorbing performance of the developed absorbers are very good thermal stability.

6 Conclusions

In summary, we demonstrated the design, fabrication and measurement of ILs-based MMAs via 3D printing technology. The impedance matching is improved by introducing a top medium with a low dielectric constant; thus, the absorber performance is significantly improved. The simulation and experimental results suggest that the absorption is over 90% at 9.26–49 GHz. Moreover, the high absorption and large bandwidth are also obtained with an oblique incidence of 0° to 45°. The main reasons for the wideband absorption have been investigated via ILs dispersion and electromagnetic resonance. Our design absorber offers a significant path for MMAs with excellent performance in ultra-wideband, polarization insensitive, and wide-angle microwave frequency ranges. The absorber has many potential applications for antennae that reduce side lobe radiation and eliminate wall reflection in anechoic chambers as well as applications in antiradar detection and stealth technology.

Acknowledgements This research was supported by the National Key Research and Development Program of China (2017YFA0403101), the Natural Science Foundation of Gansu Province (17JR5RA119), and the Fundamental Research Funds for the Central Universities (lzujbky-2018-it62, lzujbky-2018-129).

References

1. D.R. Smith, J.B. Pendry, M.C.K. Wiltshire, Metamaterials and negative refractive index. Science **305**, 788–792 (2004)
2. N. Yu, P. Genevet, M.A. Kats, F. Aieta, J.P. Tetienne, F. Capasso, Z. Gaburro, Light propagation with phase discontinuities: generalized laws of reflection and refraction. Science **334**, 333–337 (2011)
3. D. Shin, Y. Urzhumov, Y. Jung, G. Kang, S. Baek, M. Choi, H. Park, K. Kim, D.R. Smith, Broadband electromagnetic cloaking with smart metamaterials. Nat. Commun. **3**, 1213 (2012)
4. Y.M. Liu, X. Zhang, Metamaterials: a new frontier of science and technology. Soc. Rev. **40**, 2494–2507 (2011)
5. J.B. Pendry, D. Schurig, D.R. Smith, Controlling electromagnetic fields. Science **312**, 1780–1782 (2006)
6. D. Schurig, J.J. Mock, B.J. Justice, S.A. Cummer, J.B. Pendry, A.F. Starr, D.R. Smith, Metamaterial electromagnetic cloak at microwave frequencies. Science **314**, 977–980 (2006)
7. W. Li, J.G. Guan, Z.G. Sun, W. Wang, Q.J. Zhang, A near-perfect invisibility cloak constructed with homogeneous materials. Opt. Express **17**, 23410–23416 (2009)
8. N.I. Landy, S. Sajuyigbe, J.J. Mock, D.R. Smith, W.J. Padilla, Perfect metamaterial absorber. Phys. Rev. Lett. **100**, 207402 (2008)
9. M.K. Hedayati, F. Faupel, M. Elbahri, Review of plasmonic nanocomposite metamaterial absorber. Materials **7**, 1221–1248 (2014)
10. Y.X. Cui, Y.G. He, Y. Jin, F. Ding, L. Yang, Y.Q. Ye, S.M. Zhong, Y.Y. Lin, S.L. He, Plasmonic and metamaterial structures as electromagnetic absorbers. Laser Photonics Rev. **8**, 495–520 (2014)
11. Q. Chen, S.W. Bie, W. Yuan, Y.S. Xu, H.B. Xu, J.J. Jiang, Low frequency absorption properties of a thin metamaterial absorber with cross-array on the surface of a magnetic substrate. J. Phys. D. Appl. Phys. **49**, 425102 (2016)
12. X. Wang, B.Z. Zhang, W.J. Wang, J. Wang, J.P. Duan, Design, fabrication, and characterization of a flexible dual-band metamaterial absorber. IEEE Photonics J. **9**, 4600213 (2017)
13. B. Casse, W.T. Lu, Y.J. Huang, L. Menon, S. Sridhar, Super-resolution imaging using a three-dimensional metamaterials nanolens. Appl. Phys. Lett. **96**, 023114 (2010)
14. C.B. Ma, Z.W. Liu, A super resolution metalens with phase compensation mechanism. Appl. Phys. Lett. **96**, 183103 (2010)
15. C.H. Chu, M.L. Tseng, J. Chen, P.C. Wu, Y.H. Chen, H.C. Wang, T.Y. Chen, W.T. Hsieh, H.J. Wu, G. Sun, D.P. Tsai, Active dielectric metasurface based on phase-change medium. Laser Photonics Rev. **10**, 986–994 (2016)
16. W.L. Guo, G.M. Wang, T.J. Li, H.P. Li, Y.Q. Zhuang, H.S. Hou, Ultra-thin anisotropic metasurface for polarized beam splitting and reflected beam steering applications. J. Phys. D Appl. Phys. **49**, 425305 (2016)
17. Y. Wang, T.Y. Sun, T. Paudel, Y. Zhang, Z.F. Ren, K. Kempa, Metamaterial-plasmonic absorber structure for high efficiency amorphous silicon solar cells. Nano Lett. **12**, 440–445 (2011)
18. M.A. Green, S. Pillai, Harnessing plasmonics for solar cells. Nat. Photonics **6**, 130–132 (2012)
19. X.L. Liu, T. Starr, A.F. Starr, W.J. Padilla, Infrared spatial and frequency selective metamaterial with near-unity absorbance. Phys. Rev. Lett. **104**, 207403 (2010)
20. C.M. Watts, D. Shrekenhamer, J. Montoya, G. Lipworth, J. Hunt, T. Sleasman, S. Krishna, D.R. Smith, W.J. Padilla, Terahertz compressive imaging with metamaterial spatial light modulators. Nat. Photonics **8**, 605–609 (2014)
21. N. Liu, M. Mesch, T. Weiss, M. Hentschel, H. Giessen, Infrared perfect absorber and its application as plasmonic sensor. Nano Lett. **10**, 2342–2348 (2010)

22. F.N. Xia, T. Mueller, Y.M. Lin, A. Valdes-Garcia, P. Avouris, Ultrafast graphene photodetector. Nat. Nanotechnol. **4**, 839–843 (2009)
23. J.L. Percheca, Y. Desieres, N. Rochat, R. Espiau de, Lamaestre, Subwavelength optical absorber with an integrated photon sorter. Appl. Phys. Lett. **100**, 113305 (2012)
24. J.W. Park, P.V. Tuong, J.Y. Rhee, K.W. Kim, H. Jang, E.H. Choi, L. Chen, Y.P. Lee, Multi-band metamaterial absorber based on the arrangement of donut-type resonators. Opt. Express **21**, 9691 (2013)
25. D.T. Viet, N.T. Hien, P.V. Tuong, N.Q. Minh, P.T. Trang, L.N. Le, Y.P. Lee, V.D. Lam, Perfect absorber metamaterials: peak, multi-peak and broadband absorption. Opt. Commun. **322**, 209–213 (2014)
26. S. Ghosh, S. Bhattacharyya, K. Srivastava, in *Design of a Bandwidth-Enhanced Ultra Thin Metamaterial Absorber*. Progress in Electromagnetics Research Symposium Proceedings, pp. 1097–1111 (2013)
27. J. Grant, Y. Ma, S. Saha, A. Khalid, D.R.S. Cumming, Polarization insensitive, broadband terahertz metamaterial absorber. Opt. Lett. **36**, 3476–3478(2011)
28. F. Ding, Y.X. Cui, X.C. Ge, F. Zhang, Y. Jin, S.L. He, Ultra-broadband microwave metamaterial absorber. Appl. Phys. Lett. **100**, 103506 (2012)
29. S.B. Ghosh, D. Chaurasiya, K.V. Srivastava, Bandwidth-enhanced dual-band dual-layer polarization-independent ultra-thin metamaterial absorber. Appl. Phys. A. **118**, 207–215 (2015)
30. H.K. Kim, D.J. Lee, S. Lim, Frequency-tunable metamaterial absorber using a varactor-loaded fishnet-like resonator. Appl. Opt. **55**, 4113–4118 (2016)
31. J.B. Sun, L.Y. Liu, G.Y. Dong, J. Zhou, An extremely broad band metamaterial absorber based on destructive interference. Opt. Express **19**, 21155–21162 (2011)
32. J. Zhang, G. Wang, B. Zhang, T. He, Y. He, J.L. Shen, Photo-excited broadband tunable terahertz metamaterial absorber. Opt. Mater. **54**, 32–36 (2016)
33. Y.J. Yoo, S. Ju, S.Y. Park, Y.J. Kim, J. Bong, T. Lim, K.W. Kim, J.Y. Rhee, Y. Lee, Metamaterial absorber for electromagnetic waves in periodic water droplets. Sci. Rep. **5**, 14018 (2015)
34. J.W. Xie, W.R. Zhu, I.D. Rukhlenko, F.J. Xiao, C. He, J.P. Geng, X.L. Liang, R.H. Jin, M. Premaratne, Water metamaterial for ultra-broadband and wide-angle absorption. Opt. Express **26**, 5052–5059 (2018)
35. Y.Q. Pang, J.F. Wang, Q. Cheng, S. Xia, X.Y. Zhou, Z. Xu, T.J. Cui, S.B. Qu, Thermally tunable water-substrate broadband metamaterial absorbers. Appl. Phys. Lett. **110**, 104103 (2017)
36. A. Andryieuski, S.M. Kuznetsova, S.V. Zhukovsky, Y.S. Kivshar, A.V. Lavrinenko, Water: promising opportunities for tunable all-dielectric electromagnetic metamaterials. Sci. Rep. **5**, 13535 (2015)
37. X.J. Huang, H.L. Yang, Z.Y. Shen, J. Chen, H.L. Lin, Z.T. Yu, Water-injected all-dielectric ultra-wideband and prominent oblique incidence metamaterial absorber in microwave regime. J. Phys. D Appl. Phys. **50**, 385304 (2017)
38. Q.H. Song, W. Zhang, P.C. Wu, W. Zhu, Z.X. Shen, P.H.J. Chong, Q.X. Liang, Z.C. Yang, Y.L. Hao, H. Cai, H.F. Zhou, Y. Gu, G.Q. Lo, D.P.Tsai, T. Bourouina, Y. Leprince-Wang, A.Q. Liu, Water-resonator-based metasurface: an ultrabroadband and near-unity absorption. Adv. Opt. Mater. **5**, 1601103 (2017)
39. N.V. Plechkova, K.R. Seddon, Applications of ionic liquids in the chemical industry. Chem. Soc. Rev. **37**, 123–150 (2008)
40. M.J. Shiddiky, A.A. Torriero, Application of ionic liquids in electrochemical sensing systems. Biosens. Bioelectron. **26**, 1775–1787 (2011)
41. B. Leidy, M. Agudelo, M.J. Padró, R. Mario, Analysis of non-polar heterocyclic aromatic amines in beefburguers by using microwave-assisted extraction and dispersive liquid–ionic liquid microextraction. Food Chem. **141**, 1694–1701 (2013)
42. J.H. Gong, F.L. Yang, Q.F. Shao, X.D. He, X.P. Zhang, S.M. Liu, L.Y. Tang, Y.Q. Deng, Microwave absorption performance of methylimidazolium ionic liquids: towards novel ultra-wideband metamaterial absorbers. RSC. Adv. **7**, 41980–41988 (2017)
43. D. Micheli, C. Apollo, R. Pastore, M. Marchetti, X-band microwave characterization of carbon-based nanocomposite material, absorption capability comparison and RAS design simulation. Compos. Sci. Technol. **70**, 400–409 (2010)
44. S. Lee, J. Kang, C. Kim, Fabrication and design of multi-layered radar absorbing structures of MWNT-filled glass/epoxy plain-weave composites. Compos. Struct. **76**, 397–405 (2006)
45. J.G. Huddleston, A.E. Visser, W.M. Reichert, H. D.Willauer, G.A. Broker, R.D. Rogers, Characterization and comparison of hydrophilic and hydrophobic room temperature ionic liquids incorporating the imidazolium cation. Green Chem. **3**, 156–164 (2001)
46. A. Stoppa, J. Hunger, A. Thoman, H. Helm, G. Hefter, Buchner, Interactions and dynamics in ionic liquids. R. J. Phys. Chem. B **112**, 4854–4858 (2008)
47. F. Yu, J. Wang, J.F. Wang, H. Ma, H.L. Du, Z. Xu, S.B. Qu, Reflective frequency selective surface based on low-permittivity dielectric metamaterials. Appl. Phys. Lett. **107**, 211906 (2015)